Petroleum Science 18 (2021) 1427–1440

Contents lists available at ScienceDirect

Petroleum Science

journal homepage: www.keaipublishing.com/en/journals/petroleum-science

Original Paper

# A small-scale experimental study of $CO_2$ enhanced injectivity methods of the high-rank coal

Qing-He Niu [a, b], Li-Wen Cao [c, *], Shu-Xun Sang [d, **], Wei Wang [a, b], Wei Yuan [a, b], Jiang-Fang Chang [a, b], Xiao-Jun Jia [e], Wei-Min Zheng [f], Zeng-Xue Zhang [g]

[a] State Key Laboratory of Mechanical Behavior and System Safety of Traffic Engineering Structures, Shijiazhuang Tiedao University, Shijiazhuang, 050043, China
[b] Hebei Technology and Innovation Center on Safe and Efficient Mining of Metal Mines, Shijiazhuang, 050043, China
[c] School of Resource and Earth Science, China University of Mining and Technology, Xuzhou, 221008, China
[d] Jiangsu Key Laboratory of Coal-based Greenhouse Gas Control and Utilization, China University of Mining and Technology, Xuzhou, 221008, China
[e] Hebei Academy of Emergency Management, Shijiazhuang, 050081, China
[f] Hebei Iron and Steel Group Mining Co., Ltd, Tangshan, 063000, China
[g] Minmetals Mining Holding Co., Ltd, Hefei, 241000, China

ARTICLE INFO

*Article history:*
Received 6 July 2020
Accepted 29 March 2021
Available online 17 August 2021

Edited by Yan-Hua Sun

*Keywords:*
Supercritical $CO_2$
Permeability
Intermittent injection
$N_2$ displacing $CO_2$
Pre-fracturing

ABSTRACT

The attenuation of $CO_2$ injectivity has become the biggest technical barrier for the application of $CO_2$ enhanced coalbed methane recovery ($CO_2$-ECBM). Commonly, the intermittent $CO_2$ injection, $N_2$ displacing $CO_2$ and pre-fracturing are the potential $CO_2$ enhanced injectivity methods for coal reservoirs, but their mechanism and effectiveness remain to be clarified. This paper thus conducted small-scale experiments to simulate the working process of these engineering measures by an independently developed experimental device. Results show that the $CO_2$ injectivity of coal is remarkably improved by the intermittent injection mode since the $CO_2$ injection time is increased by folds and the loss of reservoir pressure can be complemented in time. The $N_2$ displacing $CO_2$ method promotes the desorption of $CO_2$ and reduces the swelling strain, with the result that the permeability of coal is improved by 74.82% and 64.95% compared with the methods of the primary subcritical $CO_2$ ($SubCO_2$) and supercritical $CO_2$ ($ScCO_2$) injection. However, the permeability reduces again with the secondary $CO_2$ injection. The permeability of the coal sample after pre-fracturing is averagely improved by 1–2 orders of magnitude, the irreversible permeability loss rate, average stress sensitivity coefficient and the permeability loss rate due to adsorption are averagely reduced by 95.885%, 61.538% and 96.297%, respectively. This indicates that the permeability of coal after pre-fracturing is no longer sensitive to both the effective stress and $ScCO_2$ adsorption, the injectivity is thus improved and stable. The $CO_2$ enhanced injectivity effects of the intermittent $CO_2$ injection, the $N_2$ displacing $CO_2$ and the pre-fracturing are various, which thus can be selected individually or jointly to improve the $CO_2$ injectivity according to the reservoir physical properties and geological conditions. This research deepens the understanding of the functional mechanism of $CO_2$ enhanced injectivity methods and provides some guidance for their selection and application in engineering practices.



## 1. Introduction

Anthropogenic greenhouse gas emissions have become the principal consideration related to the global warming, as one of the primary greenhouse gases, $CO_2$ takes an inescapable responsibility for climate change (Cheng et al., 2019; Li et al., 2015; Zhang et al., 2015). Consequently, reducing $CO_2$ emissions is gradually becoming the consensus of people. Carbon capture and sequestration (CCS) technology is an essential approach to reduce the $CO_2$ level in the atmosphere, which thus has aroused widespread

* Corresponding author.
** Corresponding author.
*E-mail addresses:* qinghniu@163.com (Q.-H. Niu), caoliwen@cumt.edu.cn (L.-W. Cao), shxsang@cumt.edu.cn (S.-X. Sang), wangweiuuu@163.com (W. Wang).

https://doi.org/10.1016/j.petsci.2021.08.006

concerns by scientists and governments around the world (Bakhshian et al., 2020; Zhao et al., 2017; Zhou et al., 2019). Currently, the depleted oil or gas reservoirs, saline aquifers and unmineable coal seams are the main geological sequestration sites (Xu et al., 2020; Zhang et al., 2017). Besides the superiority to realize geological $CO_2$ sequestration, injecting $CO_2$ into deep unmineable coal seams can also enhance coalbed methane recovery ($CO_2$-ECBM) with the displacement effect for $CH_4$, which will thus make up for the shortage of conventional energy (Ajayi et al., 2019; Niu et al. 2019a, 2020a, 2021). A large number of pilot tests have been implemented on a worldwide scale, distributing in the San Juan Basin, Illinois Basin, Williston Basin and Appalachian Basin in the United States, the Silesian coal basin in Poland, the Fenn-Big Valley in Canada, the Ishikari Coal Basin in Japan, the Qinshui Basin and Ordos Basin in China (Gunter et al., 2005; Oudinot et al., 2011; Pan et al., 2017; van Bergen et al., 2009; Yamazaki et al., 2006). However, one of the technical barriers for $CO_2$-ECBM is that the $CO_2$ injectivity is significantly lowered. As reported previously, the $CO_2$ injection rate was reduced by 40% during the initial injection stages at the Allison Unit (Reeves, 2003); a 70% reduction of the injection capability appeared during the first year of operation in the Ishikari Basin (Fujioka et al., 2010), and the loss of injection capacity was also experienced in the micro pilot field test in Qinshui Basin (Wong et al., 2007).

The most sensitive parameter influencing the $CO_2$ injectivity is permeability. It has been estimated that the low injectivity of $CO_2$ for a coal seam is caused by the reduction in permeability induced by coal swelling (Fujioka et al., 2010). For the deep unmineable coal seam, the $CO_2$ adsorption swelling of coal matrix will extend inward and compress the fracture space under the high overburden pressure, causing the attenuation of permeability in coal (Jin et al. 2019, 2020; Niu et al., 2017b; Zhou et al., 2020). The three-dimensional fracture network is extensively developed in the coal seams, mainly including the cleats developed in vertical bedding plane direction (VBD) and the bedding fractures distributed in parallel bedding plane direction (PBD) (Wang et al. 2018a, 2020a, 2020a). The structures of the two types of fractures are dynamically altered during the $CO_2$ injection process, and both of them contribute to the reduction of $CO_2$ injectivity (Niu et al., 2018). Moreover, the moisture content and temperature also affect the $CO_2$ injectivity by varying the permeability of coal (Kumar et al., 2012), but the influence level is moderate compared with the adsorption swelling of coal (Niu et al., 2019b; Wang et al., 2020b). All in all, reactions between the injected $CO_2$ and the coal matrix restrain the $CO_2$ injectivity and then affect the engineering effect of $CO_2$-ECBM.

To overcome this technical challenge, two major categories of optimizing injection scheme and coal reservoir stimulation are attempted to improve the $CO_2$ injectivity. Optimizing the injection scheme is mainly accomplished through changing the $CO_2$ injection rate or injection pressure and the composition of the injected gas, such as intermittent $CO_2$ injection (Li et al., 2016) and mixed gas injection (Fan et al., 2019). The intermittent $CO_2$ injection is often employed to enhanced oil recovery (EOR). For example, Singh (2018) compared four different injection schemes (i.e., constant rate, stepwise increasing rate, stepwise decreasing rate and cyclic rate), and considered that it would be preferable to store $CO_2$ using a cyclic injection scheme in storage reservoirs. Mixed gas injection means injecting $N_2/CO_2$ mixture or $N_2$ displacing $CO_2$, because the adsorption swelling strain induced by $N_2$ is far less than that caused by $CO_2$, the permeability loss affected by $N_2$ adsorption swelling is tiny. On this basis, Oudinot et al. (2017) considered that a larger amount of $N_2$ needs to be injected to limit the permeability loss (on the order of 85%). Other research intended to enhance $CO_2$ injectivity by improving permeability through stimulating the coal reservoir, such as hydraulic fracturing and waterless fracturing (Cao et al., 2017; Fu and Liu, 2019; Liu et al., 2021; Osiptsov, 2017). Additionally, ultrasonic wave treatment and microwave irradiation treatment are capable of improving the porosity and promoting the formation of fractures of coal (Huang et al., 2019; Shi et al. 2017, 2019). However, these methods are either limited or have not been applied to engineering practices. Up to now, few scholars have conducted experimental simulations regarding the representative enhanced $CO_2$ injectivity methods (intermittent $CO_2$ injection, $N_2$ displacing $CO_2$ and pre-fracturing). Thus, the effectiveness verifications of these methods are deficient and their functional mechanisms are uncertain, which restricts the application of $CO_2$ enhanced injectivity technologies.

Given this, the methods of intermittent $CO_2$ injection, $N_2$ displacing $CO_2$ and pre-fracturing are first simulated by an independently developed experimental device, then, the injectivity enhancement effect is verified and the functional mechanism is clarified. This research will fill the gaps in studies of $CO_2$ injectivity on coal reservoirs and provide theoretical guidance for the implementations of $CO_2$-ECBM.

## 2. Experimental

### 2.1. Sampling

#### 2.1.1. Preparation of core samples

Coal samples used were collected from Chengzhuang Coal Mine, Qinshui Basin, which is a successful commercialization area for CBM development (Li et al., 2018; Yun et al., 2012) and the target area for micro pilot tests of $CO_2$-ECBM (Pan et al., 2017). The coal blocks were obtained from the coal seams far away from the geological structural zone, which makes the samples more representative. The gathered coal blocks were wrapped by several layers of cling films and put in sampling bags to avoid the oxidation of coal surfaces. Then they were transported to the laboratory and stored in a constant temperature and humidity box.

Coal core samples with a length of 100 mm and a diameter of 50 mm were drilled from the coal blocks by a vertical drilling machine along the VBD (Fig. 1). Then the ends and profiles of samples were polished smoothly by the sandpapers. Cares were taken during the whole sample preparation process, aiming to obtain the relatively homogeneous coal samples without obvious fractures. The ASTM D2013 standard was consulted during the sampling stage. The proximate analysis, ultimate analysis and maceral composition analysis were conducted and shown in Table 1. The selected coals with maximum vitrinite reflectance ($R_{o,max}$) of 2.96% belong to high-rank coals. The size and weight were measured by a vernier caliper and a high-precision electronic balance and the results are shown in Table 2.

#### 2.1.2. Preparation of coal sample with artificial crack

To study the permeability enhancement effect by fracturing, Kumar et al. (2015) and Wu et al. (2018) proposed to simulate the fracture crack through an artificial fracture by cutting the rock core. Accordingly, the coal sample with artificial crack was prepared by the following steps: (1) A wire cutting machine was adopted to cut the coal sample in half, and the cutting surfaces were polished by abrasive papers to form an idealized crack. (2) The quartz sands with a diameter of 0.15–0.42 mm were spread evenly on the crack surface. (3) The split-cores were re-mated (sample 4) and put into the rubber sleeve of the sample cell.

### 2.2. Experimental apparatus

Fig. 2 shows a schematic diagram of the experimental apparatus used. Two gas cylinders full of He and $CO_2$ are the gas sources in this

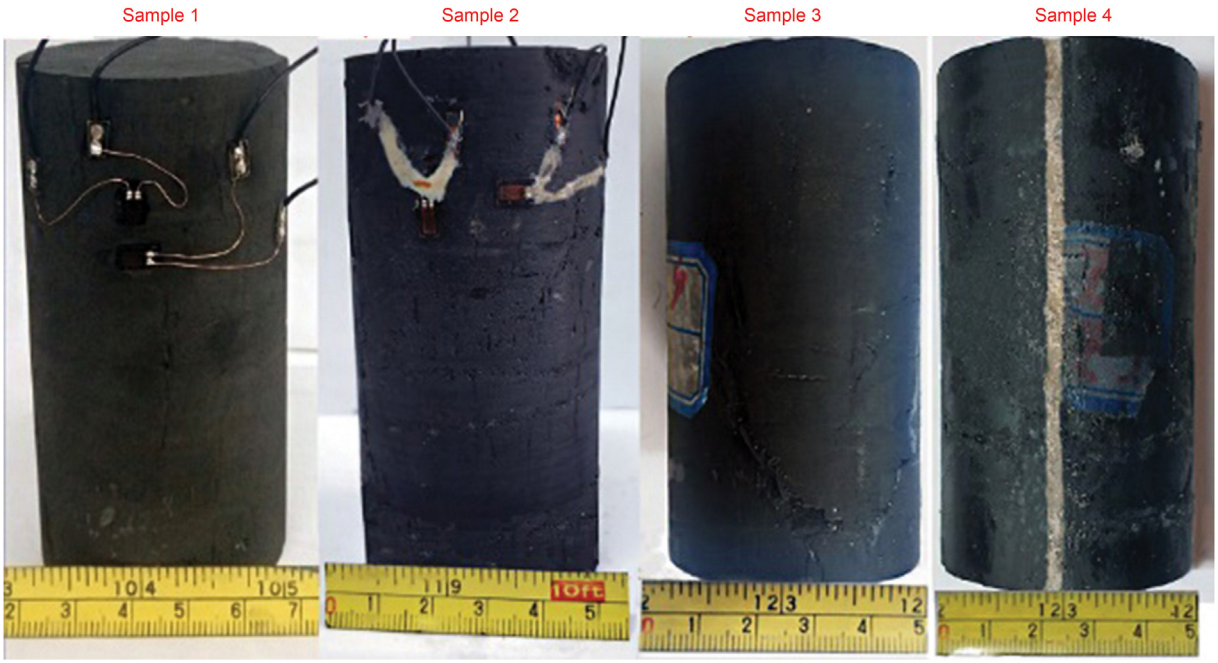


**Fig. 1.** The core samples used.

**Table 1**
Basic information of core samples taken from Chengzhuang Coal Mine.

| $R_{o,max}$, % | Proximate analysis, wt% | | | | Ultimate analysis, wt% | | | | Maceral composition, vol% | | |
|---|---|---|---|---|---|---|---|---|---|---|---|
| | $M_{ad}$ | $A_{ad}$ | $V_{daf}$ | $FC_{ad}$ | $O_{daf}$ | $C_{daf}$ | $H_{daf}$ | $N_{daf}$ | Vit | Ine | Min |
| 3.27 | 92.84 | 2.31 | 3.27 | 81.72 | 3.27 | 92.84 | 2.31 | 3.27 | 75.80 | 21.40 | 2.80 |

Note: $M_{ad}$, moisture content of air-dried basis; $A_{ad}$, ash content of air-dried basis; $V_{daf}$, volatile content of dry ash-free basis; $FC_{ad}$, fixed carbon content of air-dried basis; $O_{daf}$, oxygen content of dry ash-free basis; $C_{daf}$, carbon content of dry ash-free basis; $H_{daf}$, hydrogen content of dry ash-free basis; $N_{daf}$, nitrogen content of dry ash-free basis; Vit, vitrinite; Ine, inertinite; Min, mineral.

experiment. The gas booster is used to increase the gas pressure, the maximum target pressure can reach 30 MPa. The vacuum pump can extract the residual gases in this apparatus until the pressure in the pipeline is reduced to −0.1 MPa, providing a vacuum environment for the test. The reference cell with a volume of 5000 mL is a gas storing device, a heating system is installed in it and provides a constant temperature environment in the whole experimental process. The pressure transducer can monitor the gas pressure, with a precision of 0.01 MPa. The air compressor, oil reservoir and axial piston pump are combined to provide an axial pressure for the coal sample, the maximum normal load is 2000 kN. The syringe pump is used to provide a confining pressure for the coal sample (the maximum value is 100 MPa). The axial linear variable differential transformer (axial LVDT) and the radial LVDT with a precision of 0.1 μm are used to measure the deformation of the sample, respectively. A mass flow meter and a gas chromatograph are adopted to monitor the gas flow rate and gas component content, respectively. The experimental apparatus is controlled by built-in software on the computer, and all the data can be real-time recorded.

**Table 2**
Physical properties of coal core samples.

| Sample ID | Length, cm | Diameter, cm | Weight, g | Density, g/cm$^3$ |
|---|---|---|---|---|
| 1 | 9.784 | 4.916 | 273.672 | 1.474 |
| 2 | 9.436 | 4.966 | 259.037 | 1.412 |
| 3 | 8.604 | 4.986 | 242.281 | 1.443 |
| 4 | 8.664 | 5.048 | 252.302 | 1.456 |

### 2.3. Experimental procedure

#### 2.3.1. Experimental procedure for the continuous/intermittent $CO_2$ injection

This experiment was conducted to compare the effect of continuous and intermittent injection mode for improving the $CO_2$ injectivity. Sample 1 was used in this experiment. In the whole process, the instantaneous flow rate, injection pressure and the strain of the coal sample were real-time monitored. The experimental procedures were described as follows:

(1) Sample 1 was installed in the sample cell, and then the axial pressure and the confining pressure were increased to 12 MPa and the experimental temperature was adjusted to 35 °C.
(2) The vacuum treatment was performed with a vacuum pump for the whole device.
(3) The pneumatic valve of the reference cell and the inlet valve of the sample cell were immediately opened to introduce $CO_2$ into the sample cell. The injection pressure was kept at 4 MPa. The injection process would be stopped until the inlet flow rate dropped to zero.

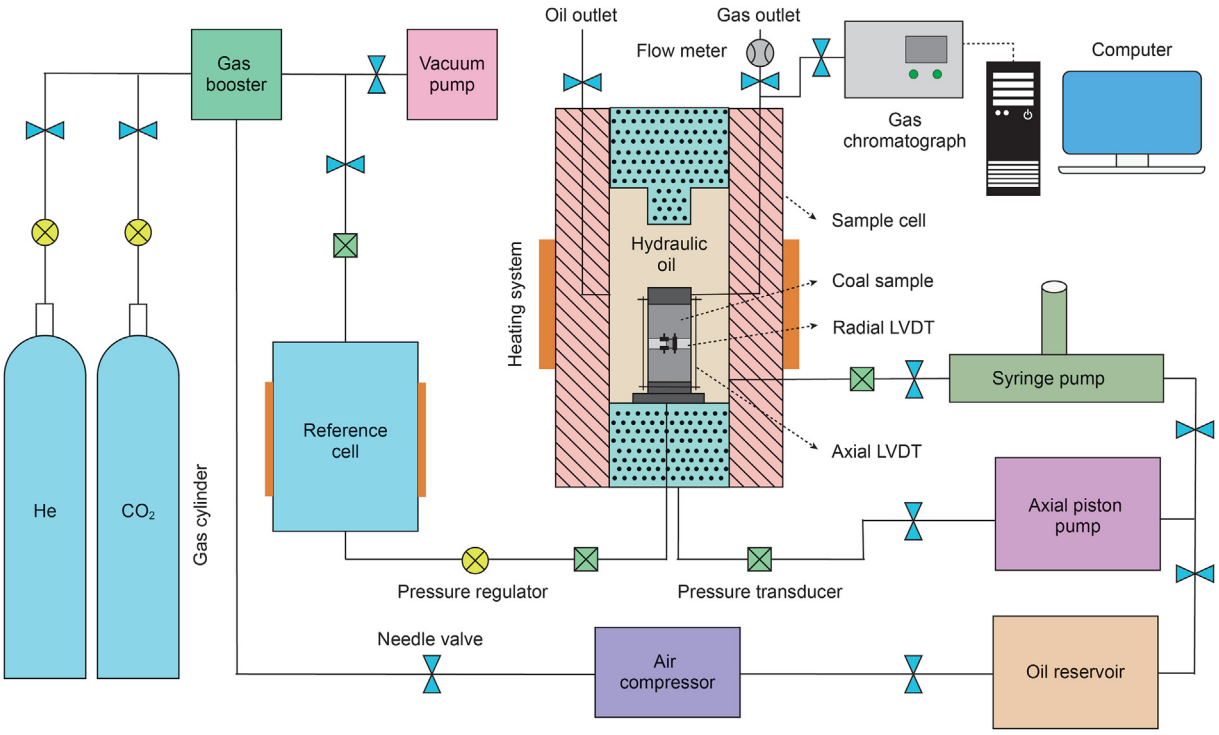


**Fig. 2.** Schematic diagram of the experimental apparatus.

(4) $CO_2$ was expulsed from the experimental device, the adsorbed $CO_2$ was extracted from the coal sample by the vacuum pump for 24 h until the desorption process was completed.
(5) $CO_2$ was injected into the sample cell at an injection pressure of 4 MPa and kept for 0.5 h. Then, the inlet valve of the sample cell was closed and the injection process was suspended for 0.5 h. The injection/stop cycle was repeated for ten times until the inlet flow rate dropped to zero;
(6) $CO_2$ was introduced into the reference cell at an injection pressure of 8 MPa, and steps (1)–(5) were repeated to accomplish the simulation of continuous/intermittent $ScCO_2$ injection.

### 2.3.2. Experimental procedure for $N_2$ displacing $CO_2$

This experiment was conducted to simulate the effect of $N_2$ displacing $CO_2$ for improving the $CO_2$ injectivity. Sample 2 was used in this test. The experimental procedures were described as follows:

(1) Sample 2 was installed into the sample cell. The axial pressure and confining pressure were increased to 12 MPa and the experimental temperature was controlled at 35 °C.
(2) The initial $N_2$ permeability of Sample 2 was measured at a confining pressure of 12 MPa, an injection pressure of 4 MPa and a back pressure of 2 MPa.
(3) After the whole device was evacuated with the vacuum pump, $CO_2$ was injected into the sample cell at an injection pressure of 4 MPa, and the strain and permeability of the coal were real-time monitored.
(4) The outlet valve was closed and $CO_2$ adsorption process was lasted for 24 h, the back pressure valve was regulated to control the outlet pressure to 2 MPa, and $N_2$ was injected to displace $CO_2$ at an pressure of 4 MPa, the strain and permeability of coal and the component content of outlet gas were dynamically monitored until the content of $N_2$ is close to 100%.
(5) When the process of $N_2$ displacing $CO_2$ was completed, $CO_2$ was reinjected into the sample cell at an pressure of 4 MPa, and the strain and permeability of coal and the component content of exit gas were recorded, until the content of $CO_2$ was close to 100%;
(6) The $N_2$ and $CO_2$ pressure were increased to 8 MPa, the back pressure was adjusted to 6 MPa, and steps (1)–(5) were repeated to conduct the experiment of $N_2$ displacing $ScCO_2$.

### 2.3.3. Experimental procedure on the enhanced $CO_2$ injectivity by pre-fracturing

The permeability of coal seams is controlled by multiple factors during the $CO_2$-ECBM process, such as $CO_2$ adsorption, effective stress, moisture, temperature and metamorphism degree (Ju et al., 2016; Meng and Li, 2013; Zhi et al., 2019), and it is commonly considered that the former two are the most crucial factors (Niu et al., 2019b). Additionally, when $CO_2$ is injected into the deep unmineable coal seam, it turns to from the subcritical $CO_2$ ($SubCO_2$) to the supercritical $CO_2$ ($ScCO_2$) when the pressure is greater than 7.4 MPa and the temperature is larger than 31 °C. Therefore, in this section, the experiment is to ascertain the different impacts of effective stress and $ScCO_2$ on the permeability of coal before and after pre-fracturing. Samples 3 and 4 were adopted to conduct this test and the flow chart is exhibited in Fig. 3. The permeability of Samples 3 and 4 under a loading/unloading cycle was measured (5 → 7→9 → 11→13 → 11→9 → 7→5 MPa for Sample 3, and 5 → 8→11 → 14→17 → 14→11 → 8→5 MPa for Sample 4), aiming to investigate the influence of effective stress on the permeability of coal before and after pre-fracturing. The $CO_2$ permeability of Samples 3 and 4 before and after $ScCO_2$ adsorption was performed at various injection pressures, aiming to probe the influence of $ScCO_2$ adsorption on the permeability of coal before

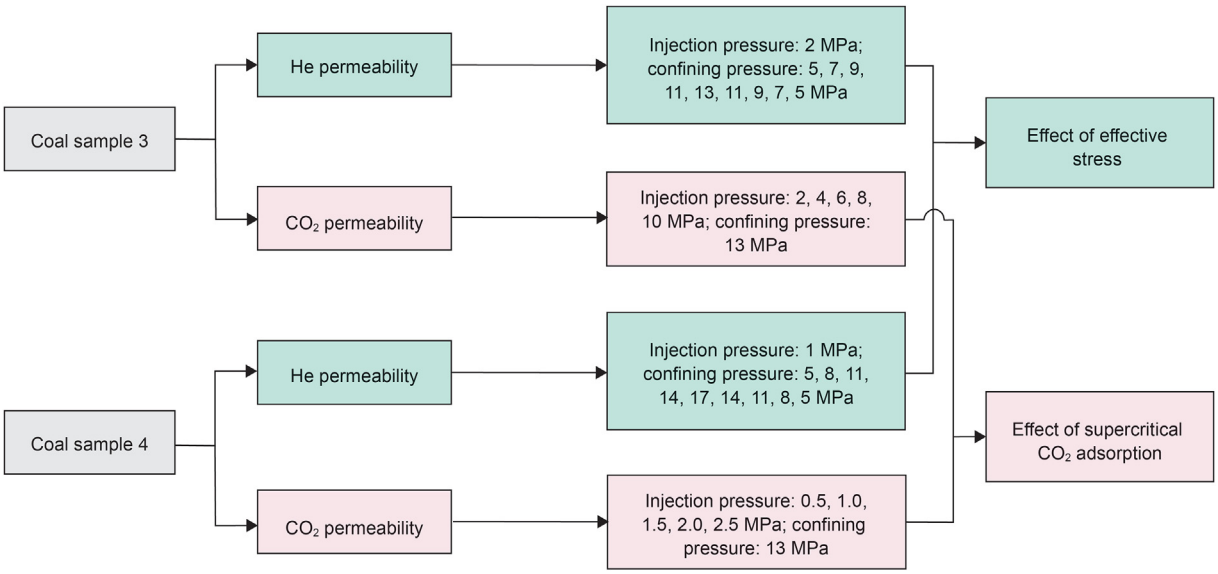


**Fig. 3.** Flow chart of permeability experiment on samples before/after pre-fracturing.

and after pre-fracturing. The adsorption time of $ScCO_2$ was 24 h, in the whole experiment, the axial pressure was 13 MPa and the experimental temperature was 35 °C. The favorable burial depth of coal seams for coalbed methane development in the Qinshui Basin is approximately 500–800 m (Shao et al., 2015), the selected experimental temperature/pressure match with the real conditions of these coal seams, according to Meng et al. (2011).

## 3. Results and discussion

### 3.1. Intermittent injection method

#### 3.1.1. Continuous/intermittent $SubCO_2$ injection

Fig. 4 shows the changes of injection pressure, confining pressure, instantaneous flow rate and volumetric strain during the continuous/intermittent $SubCO_2$ injection. During the continuous injection of the $CO_2$ into the sample at an injection pressure of 4 MPa (Fig. 4a), the instantaneous flow rate showed several fluctuations and the peak values gradually decreased at the early stage (the injection time <1.6 h). With the progressive increase in the accumulated flow rate, the adsorption swelling strain of the coal matrix appeared and elevated to 0.50%, at this time, the instantaneous flow rate of $CO_2$ was decreased to zero. This indicates that the swelling strain affected the seepage path of the coal matrix and further reduces the injectivity of the sample. The total injection volume of $CO_2$ is 1079.79 mL, the pre-calibrated free space volume is 149.70 mL, therefore, the net injection volume of $CO_2$ is 930.09 mL under the continuous $SubCO_2$ injection mode.

For the intermittent $SubCO_2$ injection mode, ten injection/stop cycles were conducted, and the interval time was 0.5 h. Fig. 4b shows that the instantaneous flow rate of $CO_2$ increased to a peak value quickly when the entrance valve was opened, and then it was rapidly attenuated. When the entrance valve was closed, the instantaneous flow rate was reduced gradually, and the $CO_2$ pressure also decreased because the adsorption process was continued. With the increase in the number of injection/stop cycles, the peak value of the instantaneous flow rate gradually decreased, and it reduced to zero when the volumetric strain reached 0.60%. The total injection volume of $CO_2$ is 1301.15 mL, and the net injection volume of $CO_2$ is 1151.45 mL after deducting the free space volume under the intermittent $SubCO_2$ injection mode. The net $SubCO_2$ injection volume by intermittent injection mode is improved by 23.80%, compared with that by continuous injection mode.

#### 3.1.2. Continuous/intermittent $ScCO_2$ injection

The experimental results of continuous/intermittent $ScCO_2$ injection are shown in Fig. 5. As can be seen from Fig. 5a, after the injection of $ScCO_2$ at 8 MPa, the instantaneous flow rate of $CO_2$ also

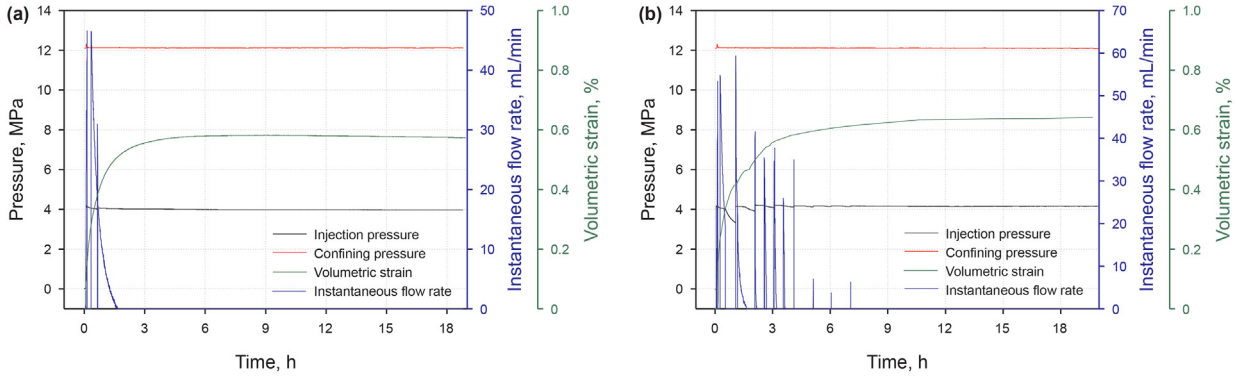


**Fig. 4.** Experimental results of continuous/intermittent injection of $SubCO_2$ into the sample. (**a**) Continuous injection, and (**b**) intermittent injection.

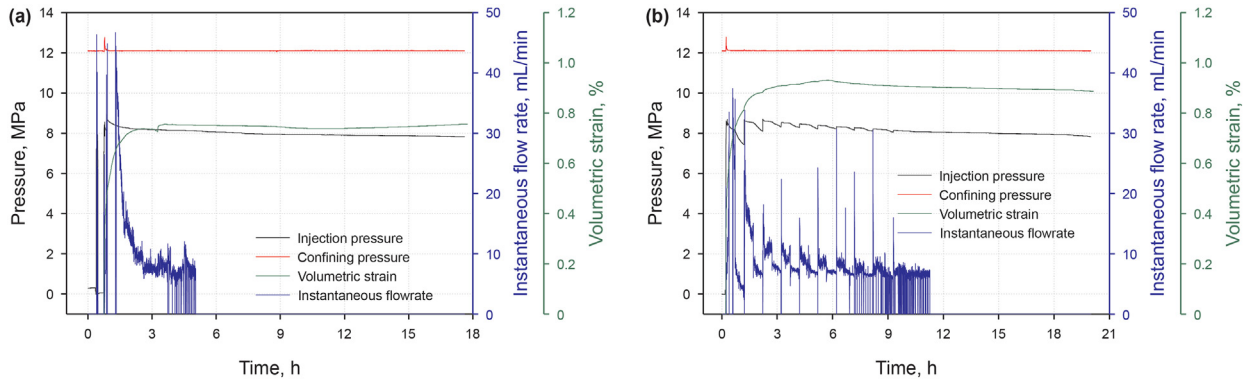


**Fig. 5.** Experimental results of continuous/intermittent injection of $ScCO_2$ into the sample. (**a**) Continuous injection, and (**b**) intermittent injection.

presented several fluctuations, however, unlike the $SubCO_2$ injection, the injection time became longer, and the instantaneous flow rate reduced to zero when the injection time was equal to 5 h. The time when the maximum volumetric swelling strain is reached was earlier than the time when the instantaneous flow dropped to zero. Although the adsorption swelling deformation reduced the injectivity of $CO_2$, the injection process was extended if the $CO_2$ injection pressure was high enough. The total injection volume of $CO_2$ was 2622.85 mL, and the net injection volume of $CO_2$ was 2323.45 mL under the continuous injection mode after deducting the free space volume.

For Fig. 5b, the instantaneous flow rate of $CO_2$ has not decreased to zero during the process of ten injection/stop cycles, which was different from the continuous $ScCO_2$ injection mode. The intermittent injection mode largely lengthened the injection process, manifesting in that the injection time of intermittent $ScCO_2$ injection was 2.25 times that of the continuous $ScCO_2$ injection. Additionally, although the intermittent injection mode was widely adopted, the effects of $SubCO_2$ and $ScCO_2$ were different. For the intermittent $SubCO_2$ injection, the sample seemed almost impossible to be injected at the seventh injection/stop cycle; however, for the intermittent $SubCO_2$ injection, the injection process continued for 1.96 h after ten injection/stop cycles. Through the intermittent injection mode, the total injection volume of $CO_2$ was 5297.45 mL, the net injection volume of $CO_2$ was 4998.05 mL after deducting the free space volume. The net injection volume of $ScCO_2$ was improved by 115.11% by intermittent injection mode, compared with the continuous injection mode.

#### 3.1.3. Mechanism of intermittent injection to enhance $CO_2$ injectivity

The above analysis shows that the $CO_2$ pressure is gradually decreased when $CO_2$ injection is ceased. For the $CO_2$-ECBM pilot test, when the injection volume of $CO_2$ reaches the maximum storage capacity of the coal reservoir, the free $CO_2$ is regarded as the gas source of the coal reservoir when the injection well is closed. As the $CO_2$ adsorption continued, the volume of free $CO_2$ in the coal reservoir was reduced gradually, causing a decrease in reservoir pressure. The $CO_2$ was re-injected into the coal reservoir when the injection well was opened, hereof, the pressure difference appeared, which further promoted the adsorption of $CO_2$. With the increase in the injection/stop cycles, the cumulative injection volume of $CO_2$ was accreted gradually. In brief, the intermittent injection mode offsets the pressure loss during the shutting-in process of the injection well and results in the increase in $CO_2$ injectivity for the coal reservoir.

Also, the $CO_2$ injection time is prolonged through intermittent injection mode. For the $SubCO_2$ and $ScCO_2$, the injection times of intermittent injection were 4.44 and 2.25 times of continuous injection. The extension of the injection process by intermittent injection mode is due to that the permeability of the coal reservoir can be recovered in the injection interruption period, which can be authenticated from the field engineering practices. For instance, Dutta and Zoback (2012) found that the loss of permeability can partially be overcome by intermittent injection for 6 months followed by a soak period. The extended injection process can provide sufficient time for $CO_2$ to flow and store in the coal matrix thoroughly, causing the improvement of $CO_2$ injectivity.

All in all, the intermittent injection possesses the following advantages: (1) compensating the loss of reservoir pressure by continuous injection; (2) prolonging the injection process of $CO_2$; (3) promoting the permeability recovery during the shut-in period. It enlightens us that the intermittent $CO_2$ injection is a potential and effective enhanced $CO_2$ injectivity method.

### 3.2. $N_2$ displacing $CO_2$ method

#### 3.2.1. Variation of gas components during $N_2$ displacing $CO_2$

Fig. 6 shows the variations of gas component content during the processes of the primary $SubCO_2$ injection, $N_2$ displacing $SubCO_2$ and the second $SubCO_2$ injection. When the experimental time was 1.47 h, $SubCO_2$ at an injection pressure of 4 MPa was introduced into the whole device, $CO_2$ content monitored at the end of the device was above 99%, but it did not reach 100%, which is because that the $CO_2$ concentration in the purchased gas cylinder is 99.9% and a minor error existed. Then the $CO_2$ adsorption process started and continued for 24.67 h, which can be considered that the adsorption equilibrium has been reached (Dutta and Zoback. 2012). When the experiment proceeded to 26.14 h, $N_2$ was injected into the sample cell at an injection pressure of 4 MPa, and the displacement process began. The gas composition changed periodically, i.e., (1) When experimental time fell in the range of 26.14–29.71 h, the $CO_2$ content rapidly reduced from 99.37% to 8.13% and the $N_2$ content sharply raised from 0.63% to 91.87%, which indicated that the injection of $N_2$ start to displace the pre-adsorbed $CO_2$. (2) When the experimental time ranged from 29.71 h to 37.24 h, similarly, the $CO_2$ content decreased (from 8.13% to 1.55%) and the $N_2$ content increased (from 91.87% to 98.45%), while the whole trend was quite slow. During the time segment of 37.24–45.03 h, the gas content changed slightly and essentially tended to be constant. Subsequently, the $SubCO_2$ was re-injected into the coal sample at 45.74 h, resulting in the re-increase of $CO_2$ content and the re-decrease of $N_2$ content.

The changes in gas component content in the processes of the

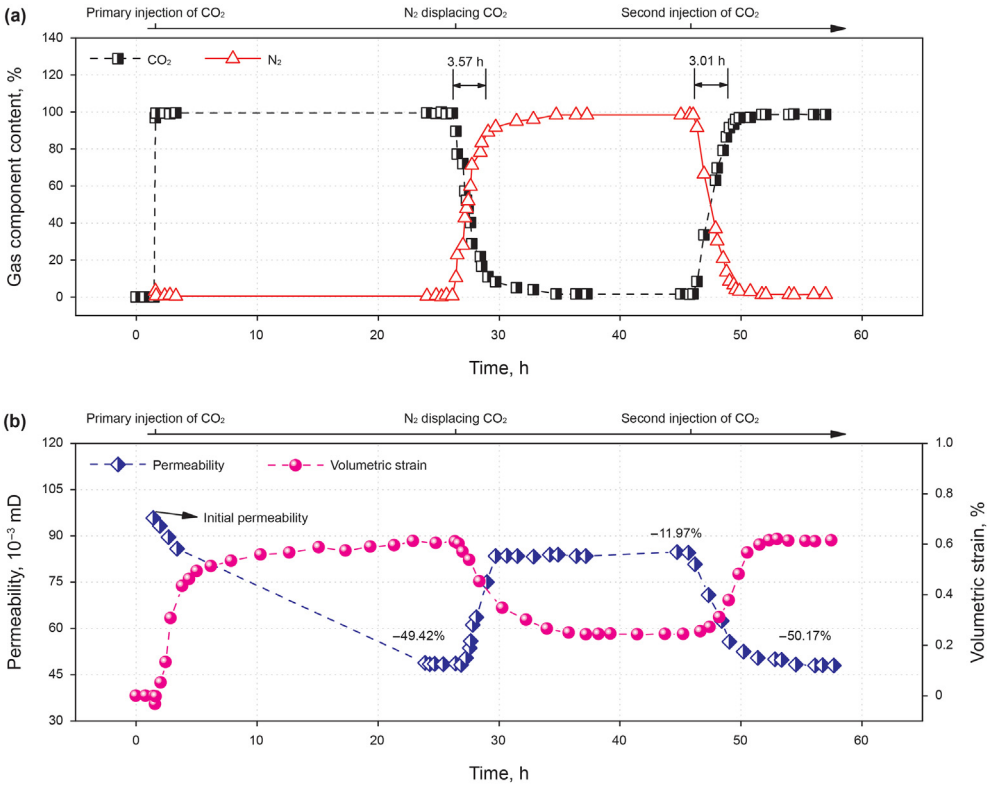


**Fig. 6.** Gas component content, permeability and volumetric strain of coal in the processes of the primary $SubCO_2$ injection, $N_2$ displacing $SubCO_2$, and the second $SubCO_2$ injection.

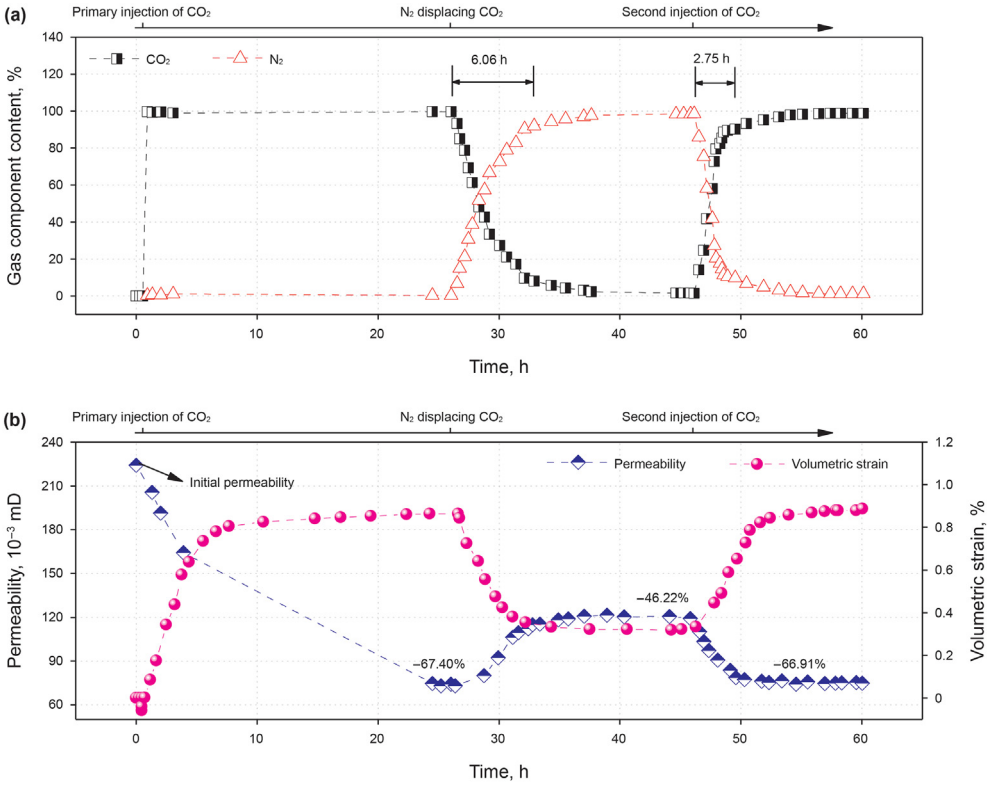


**Fig. 7.** Gas component content, permeability and volumetric strain of coal in the processes of the primary $ScCO_2$ injection, $N_2$ displacing $ScCO_2$ and the second $ScCO_2$ injection.

primary $ScCO_2$ injection, $N_2$ displacing $ScCO_2$ and the second $ScCO_2$ injection are shown in Fig. 7. The $ScCO_2$ was injected into the sample cell at the pressure of 8 MPa when the experimental time was equal to 0.55 h, the $CO_2$ content reached the maximum value, and then $N_2$ was injected at 8 MPa to displace $ScCO_2$. The $CO_2$ content decreased and the $N_2$ content increased, the gas content changed expeditiously at the experimental time of 26.06–30.63 h and changed slowly at the experimental time of 30.63–37.64 h, showing a phased evolution law. Thereafter, the $ScCO_2$ was re-injected into the coal sample, and the $CO_2$ content reached the maximum again.

The experiment in this section shows that in the processes of $CO_2$ injection, $N_2$ displacing $CO_2$ and second $CO_2$ injection, the evolutionary trends of gas content are analogous, regardless of the phase state of $CO_2$. Nevertheless, there exists differences in the displacement time and displacement efficiency. The displacement time was 3.57 h when the $CO_2$ content decreased to 10% for $N_2$ displacing $SubCO_2$, and at the same conditions, the displacement time reached 5.55 h for $N_2$ displacing $ScCO_2$, indicating that it was more difficult for $N_2$ displacing $ScCO_2$. For the second $SubCO_2$ injection, the duration when the $CO_2$ content increased to 90% was 3.01 h, and at the same conditions, the duration reduced to 2.75 h for the second $ScCO_2$ injection.

The gas adsorption capacity follows the sequence: $ScCO_2 > SubCO_2 > N_2$, therefore, $ScCO_2$ will be the winner during the competitive adsorption process, which manifests in the phenomena that $ScCO_2$ molecules rapidly supersedes $N_2$ molecules and occupy their adsorption sites with the higher efficiency.

Fractures in the coal are mainly seepage passages, and pores in the coal are the adsorption and diffusion sites for gas (Chen et al., 2021). Comparing with the displacement effect of $CH_4$ by $CO_2$, $N_2$ displacing $CO_2$ is more close to the flushing process. Before the injection of $N_2$, the $CO_2$ adsorption is in equilibrium, and the $CO_2$ pressure in the fractures is equal to that in the coal matrix when $N_2$ is injected into the coal, the total gas pressure in the fractures is composed of $CO_2$ partial pressure ($p_1$) and $N_2$ partial pressure ($p_2$). With the continuous injection of $N_2$, $p_2$ increases and $p_1$ decreases. When $p_2 > p_1$, $CO_2$ is flushed out of the coal under the action of gas pressure difference, accompanied by the approximate linear reduction of $CO_2$ content. When the $CO_2$ content in the fractures is less than that in the coal matrix, $CO_2$ is desorbed and diffused from the coal matrix to the fractures under the action of gas concentration difference, and finally, $N_2$ displacing $CO_2$ is completed. In this stage, the $CO_2$ content is reduced slowly.

Figs. 6 and 7 also illustrate the volumetric deformation of coal occurred in the processes of the primary $CO_2$ injection, $N_2$ displacing $CO_2$ and second $CO_2$ injection. For Fig. 6, during the primary $SubCO_2$ injection, the volumetric strain reduced instantaneously to −0.03%, which reflects the global compression effect of $CO_2$ for the coal body. The swelling strain induced by the $SubCO_2$ adsorption increased with the increase of experimental time, the maximum swelling strain reached 0.59%. During the $N_2$ displacing $SubCO_2$, the desorption of $CO_2$ caused the matrix shrinking of coal (Niu et al., 2017a), although $N_2$ adsorption also resulted in matrix swelling, the ultimate swelling strain was still reduced to 0.25%, which was greater than the initial strain value. And during the second $SubCO_2$ injection, the coal matrix swelled again and the maximum swelling strain reached 0.61%, nearly equaling to the swelling strain induced by the primary $SubCO_2$ injection.

For Fig. 7, the changes of the volumetric strain of coal occurred in the processes of the primary $ScCO_2$ injection, $N_2$ displacing $ScCO_2$ and the second $ScCO_2$ injection were similar to those of $SubCO_2$, but the values of swelling strain varied. During the primary $ScCO_2$ injection, the maximum swelling strain of the coal was 0.84%, which was higher than that induced by $SubCO_2$ adsorption. When $N_2$ was injected into the coal saturated with $ScCO_2$, the coal shrank and the volumetric strain decreased to 0.32%. Similarly, when $ScCO_2$ was injected into the coal again, the volumetric strain re-increased to 0.87%. The deformation of the coal body is closely related to the adsorption/desorption of gas ($SubCO_2$/$ScCO_2$ and $N_2$), and the difference in adsorption capacity of various types of gases is the fundamental cause of the dynamic changes of the swelling strain of the coal during the primary $CO_2$ injection, $N_2$ displacing $CO_2$ and the second $CO_2$ injection.

### 3.2.2. Variation of permeability of coal during $N_2$ displacing $CO_2$

Generally, the gas flow in coal is laminar (Chao et al., 2019; Gao et al., 2017; Sharma et al., 2017). Thus, Darcy's law was used to calculate the permeability of the sample from the measured steady-state flow rates (Ranjith et al., 2011):

$$k = \frac{2Qp_0\mu L}{A(p_i^2 - p_0^2)} \tag{1}$$

where $Q$, $\mu$, $p_i$, and $p_0$ are the gas flow rate, the gas viscosity, the inlet gas pressure and outlet gas pressure, respectively; $A$ and $L$ are the cross-sectional area and the length of the core sample, respectively; $k$ is the permeability of the sample. In the processes of the primary $CO_2$ injection and the second $CO_2$ injection processes, the $CO_2$ is adopted to calculate the permeability of coal, while, the $N_2$ is used to measure the permeability of the coal in the $N_2$ displacing $CO_2$ process.

The permeability evolution of the coal is what we are most concerned about in the processes of the primary $CO_2$ injection, $N_2$ displacing $CO_2$ and the second $CO_2$ injection. Corresponding results are shown in Figs. 6 and 7. As can be seen from Fig. 6, the initial coal permeability at an injection pressure of 4 MPa was $95.78 \times 10^{-3}$ mD when the experimental time exceeded 1.47 h. When the $SubCO_2$ was continuously injected in coal, the coal permeability was gradually attenuated to $48.45 \times 10^{-3}$ mD, with the decrease percentage of 49.42%; when $N_2$ was injected into the coal saturated with $SubCO_2$, the coal permeability was gradually recovered to $84.70 \times 10^{-3}$ mD at the experimental time of 44.72 h, which was promoted by 74.82% compared with the permeability in the primary $SubCO_2$ injection. After that, the second $SubCO_2$ injection induced a decrease in coal permeability once again, the minimum value was $48.05 \times 10^{-3}$ mD, and the permeability reduced by 50.17% compared with the initial value.

For Fig. 7, the permeability of the coal under conditions of the primary/second $ScCO_2$ injection and $N_2$ displacing $ScCO_2$ also showed the same variation law. The initial permeability of the coal at 4 MPa injection pressure was $224.18 \times 10^{-3}$ mD, the primary $ScCO_2$ injection lowered the permeability to $73.09 \times 10^{-3}$ mD with a reduction of 67.40%; the $N_2$ displacing $ScCO_2$ recovered the permeability to $120.56 \times 10^{-3}$ mD, and the coal permeability was increased by 64.95% compared with the permeability at the primary $ScCO_2$ injection; however, the coal permeability reduced to $74.18 \times 10^{-3}$ mD with the second $ScCO_2$ injection, approaching to that in the primary $ScCO_2$ injection.

The simulation experiments indicated that $N_2$ displacing $CO_2$ indeed promoted the recovery of permeability in the coal, nevertheless, its permeability recovery rate (64.95%) was lower than that of $N_2$ displacing $SubCO_2$ (74.82%), which may be related to the various difficulties of $N_2$ displacing $CO_2$ at different phase states. The permeability enhancement effect of coal seams by $N_2$ displacing $CO_2$ has been reported in previous research, e.g., Zhang et al. considered that the permeability was improved by 73.51%–106.61% after $N_2$ displacement at a gas pressure of 5–14 MPa (Zhang et al., 2018); for the $CO_2$-ECBM field test in Ishikari basin, the injection of $N_2$ increased the daily injection rate of $CO_2$ more than four times

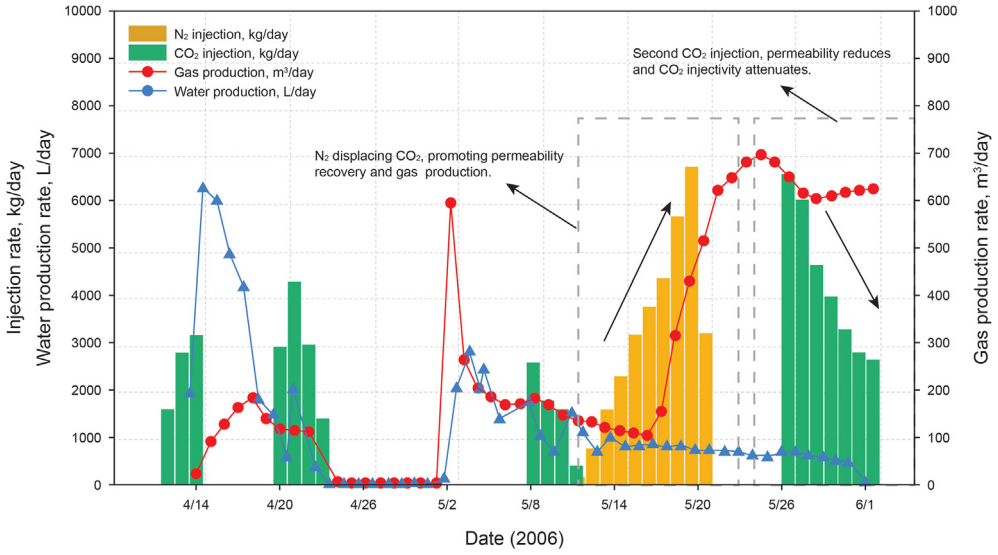


**Fig. 8.** Production and injection curves from the pilot test of $CO_2$-ECBM (Fujioka et al., 2010).

(Fujioka et al., 2010) (Fig. 8), however, this positive effect was only temporary, once the $CO_2$ was reinjected, the $CO_2$ injectivity still reduced slowly. This can be verified by simulation experiments in this section, i.e., the second $CO_2$ injection has conversely driven $N_2$ out of the sample, and decreased the permeability to the level of the primary $CO_2$ injection.

### 3.2.3. Mechanism of $N_2$ displacing $CO_2$ to enhance $CO_2$ injectivity

In the $CO_2$-ECBM field project, there exists an interaction of three gases after $N_2$ injection, i.e., $CO_2$, $CH_4$ and $N_2$. Because the adsorption capacities of coal for different gases are quite different, the gas composition in the coal continuously changes. Based on the kinetic equation of multicomponent gas adsorption, this process can be expressed as (Ji, 2015):

$$\frac{\mathrm{d}x}{\mathrm{d}t} = \eta_v \theta_{N_2} \theta_{CH_4} \theta_{CO_2} = \frac{\eta_v b_{N_2} b_{CH_4} b_{CO_2} p_{N_2} p_{CH_4} p_{CO_2}}{\left(1 + b_{N_2} p_{N_2} + b_{CH_4} p_{CH_4} + b_{CO_2} p_{CO_2}\right)^2} \tag{2}$$

where $\mathrm{d}x/\mathrm{d}t$ is the gas displacement/desorption rate; $\eta_v$ is the gas displacement/desorption constant; $\theta_{N_2}$, $\theta_{CH_4}$ and $\theta_{CO_2}$ are respectively the coverage rate of $N_2$, $CH_4$ and $CO_2$ at adsorption equilibrium; $b_{N_2}$, $b_{CH_4}$ and $b_{CO_2}$ are the adsorption constants of $N_2$, $CH_4$ and $CO_2$, respectively; $p_{N_2}$, $p_{CH_4}$ and $p_{CO_2}$ are the partial pressure of $N_2$, $CH_4$ and $CO_2$ respectively.

Because the adsorption capacity of coal for $N_2$ is lower than those of $CH_4$ and $CO_2$, Equation (2) can be simplified by using the inequality of $b_{N_2} p_{N_2} \ll 1 + b_{CH_4} p_{CH_4} + b_{CO_2} p_{CO_2}$ as:

$$\frac{\mathrm{d}x}{\mathrm{d}t} = \frac{\eta_v b_{N_2} b_{CH_4} b_{CO_2} p_{N_2} p_{CH_4} p_{CO_2}}{\left(1 + + b_{CH_4} p_{CH_4} + b_{CO_2} p_{CO_2}\right)^2} \tag{3}$$

Equation (3) shows that the $N_2$ injection promotes the partial pressure of $N_2$ and enhances the desorption rate of $CH_4$ and $CO_2$. The desorption process is accompanied by the matrix shrinking effect, which results in the expansion of narrow fractures or reopening of closed fractures, and thus the permeability of the coal is promoted. The ameliorated permeability accelerates the entrance of $CO_2$ into coal pores by seepage-diffusion-adsorption effects, which is in favor of $CO_2$-ECBM. However, during the process of $N_2$ displacing $CO_2$, the discharge of the desorption $CO_2$ will reduce the $CO_2$ storage capacity, which counts against the purpose of $CO_2$ geological sequestration.

## 3.3. Pre-fracturing method

### 3.3.1. Influence of effective stress on the permeability of coals before/after pre-fracturing

Generally, the coal permeability decreases under loading conditions and increases under unloading conditions, but it is almost impossible to completely recover the permeability to the initial level. According to the description by Meng and Li (2013), the irreversible permeability loss rate ($R_{ip}$) under a loading/unloading cycle is defined as:

$$R_{ip} = \frac{k_0 - k_0'}{k_0} \times 100\% \tag{4}$$

where $R_{ip}$ is the irreversible permeability loss rate, $k_0$ represents the initial permeability of the sample; $k_0'$ represents the permeability of the sample after a loading/unloading cycle. Generally, the stress sensitivity coefficient ($\alpha_k$) is always adopted to characterize the stress sensitivity of coal reservoir (Geng et al., 2017), and defined as follows:

$$\alpha_k = -\frac{1}{k_0}\frac{\partial k}{\partial \sigma} \tag{5}$$

where $k$ represents the permeability; $k_0$ represents the initial permeability; $\sigma$ represents the confining pressure. Moreover, the permeability of a reservoir is verified to be highly susceptible to stress and has been confirmed by scholars in experiments to generally decrease exponentially with the increase in effective stress (Geng et al., 2017; Wang et al., 2018b; Zou et al., 2016):

$$k = k_0 \mathrm{e}^{-3C_f(\sigma_h - \sigma_{h0})} \tag{6}$$

where $C_f$ is the fracture compression coefficient; $\sigma_h$ is the external stress and $\sigma_{h0}$ is its initial value.

Fig. 9 shows the measured permeability of coal samples before/after pre-fracturing, every measurement was conducted twice to ensure data accuracy. For the coal sample before pre-fracturing, the increase in the effective stress decreased its permeability and the

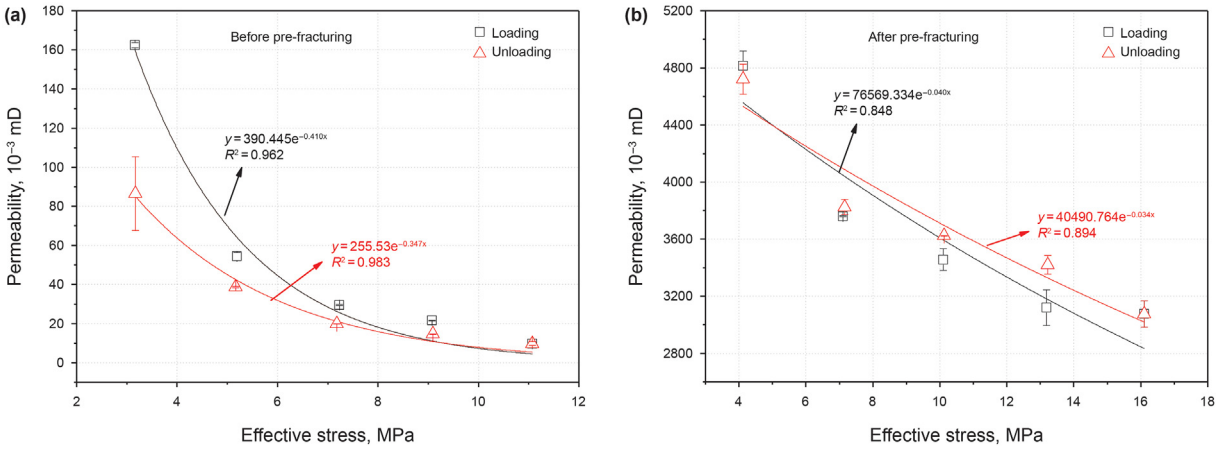


**Fig. 9.** Relationship between permeability and effective stress of samples before and after pre-fracturing.

decrease in the effective stress recovers its permeability, which was consistent with previous experimental results (Jiang et al., 2017; Ye et al., 2017; Zou et al., 2016). However, the permeability curve of the coal after pre-fracturing showed a huge difference, the curve almost changed to be straight-line though it still can be fitted by the exponential function (Eq. (6)) with higher $R^2$. Additionally, in some cases, the permeability at the unloading stage was larger than that at the loading stage. The pre-fracturing treatment for samples affected its evolution of permeability.

For the loading stage, the permeability of the coal before pre-fracturing ranged from 109.331 $\times$ $10^{-3}$ mD to 10.223 $\times$ $10^{-3}$ mD, and that of the coal after pre-fracturing fell in the range of 4812.750 $\times$ $10^{-3}$ to 3076.614 $\times$ $10^{-3}$ mD; for the unloading stage, the coal permeability ranged from 9.785 $\times$ $10^{-3}$ mD to 86.512 $\times$ $10^{-3}$ mD before pre-fracturing, and 3076.614 $\times$ $10^{-3}$ mD and 4720.176 $\times$ $10^{-3}$ mD after pre-fracturing. It can be seen that the pre-fracturing treatment for the coal improved the permeability by 1–2 orders of magnitude. Although previous scholars have also confirmed that the permeability increases after pre-fracturing, the increasing magnitude was variously reported in different pieces of literature, e.g., Kumar et al. demonstrated that when the monolayer proppant was sandwiched in the coal fracture, the He permeability may be as high as ~10 fold than the initial value (Kumar et al., 2015); Wu et al. considered that the permeability of the proppant supported fracture was 2–3 orders of magnitude higher than that of the original sample; and for shale (Wu et al., 2018), Tan et al. (2017) deemed that the permeability of propped fractures was about a few hundred or even a few thousand times higher than those of natural fractures. The increasing magnitude of permeability depended on the proppant packing pattern, the layer number, particle size and the type of proppant. Generally, the hardness of proppant affects the compressibility of fractures and then influences the permeability of the coal sample; increasing the proppant layer, enlarging the proppant particle size and making the packing pattern sparse can create more space for the flow of gas, and thus, the permeability enhancement effect induced by pre-fracturing will be superior. In conclusion, there is no doubt that the pre-fracturing method is capable of dramatically enhancing the permeability of coal reservoirs.

The irreversible permeability loss rate and average stress sensitivity coefficient were calculated according to Eqs. (4) and (5). The average irreversible permeability loss rate of coal samples before and after pre-fracturing were 46.775% and 1.925%, respectively, and the pre-fracturing has reduced the irreversible permeability loss rate by 95.885%; the average stress sensitivity coefficient of the sample before and after pre-fracturing were 0.117 and 0.045, respectively, and the pre-fracturing has lowered the average stress sensitivity coefficient by 61.538%. The irreversible permeability loss rate and the average stress sensitivity coefficient of coal samples after pre-fracturing were largely weakened, and it can be deduced that the permeability of the coal is insensitive to the effective stress after pre-fracturing treatment. The main reason can be attributed to that the stiffness of quartz sand is far greater than that of the coal matrix. Under the acting of effective stress, the quartz sand is hard to be compressed, it thus supports the fractures in coal and provides adequate seepage spaces for gas. Consequently, the high-permeability and low-stress sensitivity properties of the ameliorated coal reservoirs are highly favorable for $CO_2$ injection.

### 3.3.2. *Influence of $ScCO_2$ adsorption on the permeability of coals before/after pre-fracturing*

The adsorption swelling behavior affects the permeability in coal (Jia et al., 2018; Niu et al., 2017b; Wei et al., 2019), the seepage paths are cramped and the permeability is reduced through the physicochemical reaction between the $CO_2$ and coal. Based on the permeability pre and post the $CO_2$ adsorption, the parameter of permeability loss rate due to adsorption was defined as (Niu et al., 2019b):

$$R_a = \frac{k_0 - k_a}{k_0} \times 100\% \quad (7)$$

where $k_0$ represents the initial permeability of the coal sample, and $k_a$ is the permeability of the coal sample when the $CO_2$ adsorption equilibrium state is reached.

The permeability changes of samples without/with pre-fracturing treatment before and after $ScCO_2$ adsorption are shown in Fig. 10. The permeability after $ScCO_2$ adsorption was lower than that before $ScCO_2$ adsorption, indicating that the adsorption swelling narrows the fractures and reduced the coal permeability. Nevertheless, the permeability of pre-fractured core sample did not show apparent permeability attenuation after $ScCO_2$ adsorption, and even some permeability values were larger than that of the sample without $ScCO_2$ adsorption. Based on Eq (7), the permeability loss rate due to adsorption of coal samples before and after pre-fracturing was obtained (Fig. 10). The pre-fracturing also decreased the permeability loss rate due to adsorption of the coal sample, manifesting in the fact that the average permeability loss rate due to adsorption of the pre-fractured core sample was lowered by 96.297% of the primary sample.

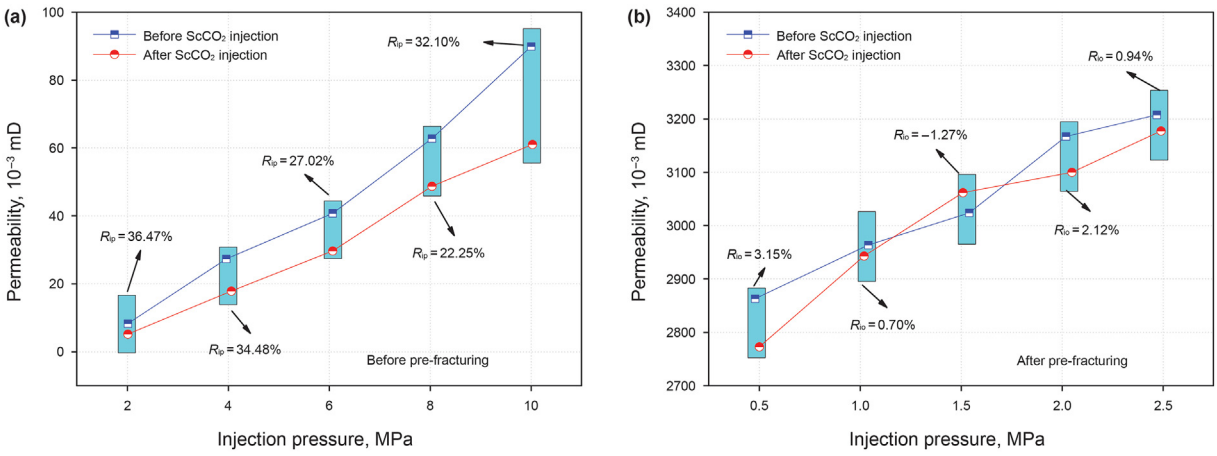


**Fig. 10.** The permeability loss rate due to adsorption of coal samples before and after pre-fracturing.

The decrease of permeability loss rate due to adsorption indicates that the permeability of the coal sample after pre-fracturing is also insensitive to $ScCO_2$ adsorption. This is because the quartz sand with higher stiffness can withstand the wall of fractures, increasing the difficulty for swelling deformation developing to the interior of fractures. Simultaneously, even if the fracture structure may also be influenced by adsorption swelling, this effect can be negligible due to the sharp increase in the permeability of coal after pre-fracturing.

### 3.3.3. *Mechanism of pre-fracturing to enhance $CO_2$ injectivity*

As described in the literature (Niu et al., 2020b), for $CO_2$-ECBM, $CO_2$ flows from the injection well, tectonic fractures or bedding plane fractures, cleats, and finally is adsorbed in the multiscale pores of coal. For structure-undeveloped coal seams (e.g., coal seams in the Qinshui Basin), the bedding plane fractures and cleats all control the $CO_2$ injection because it is a continuous process (Perera et al., 2013). Research indicated that the bedding plane seepage is mainly controlled by effective stress, contrarily, the cleat seepage is mainly affected by the adsorption of $ScCO_2$ (Niu et al., 2018).

The diagrammatic sketch of coal seams modified by fracturing is shown in Fig. 11. After fracturing, abundant crisscross cracks are induced in coal reservoirs. The cracks in the PBD enlarge the seepage space of $CO_2$, and cracks in the VBD link the cleats and increase its connectivity, then the global permeability of the coal seam is largely improved. When water, sand and additives are pumped under pressure into the coal seam, the fracturing sands are filled in the primary fractures and epigenetic cracks. As discussed above, the permeability stress sensitivity in the PBD and the permeability loss rate due to adsorption of fractures in the VBD all drop sharply. This means that the permeability of coal seams after pre-fracturing is independent of the effective stress and $ScCO_2$ adsorption, as the two factors are the main controlling factors for the permeability, we thus can consider the $CO_2$ injectivity is promoted evidently by the pre-fracturing method.

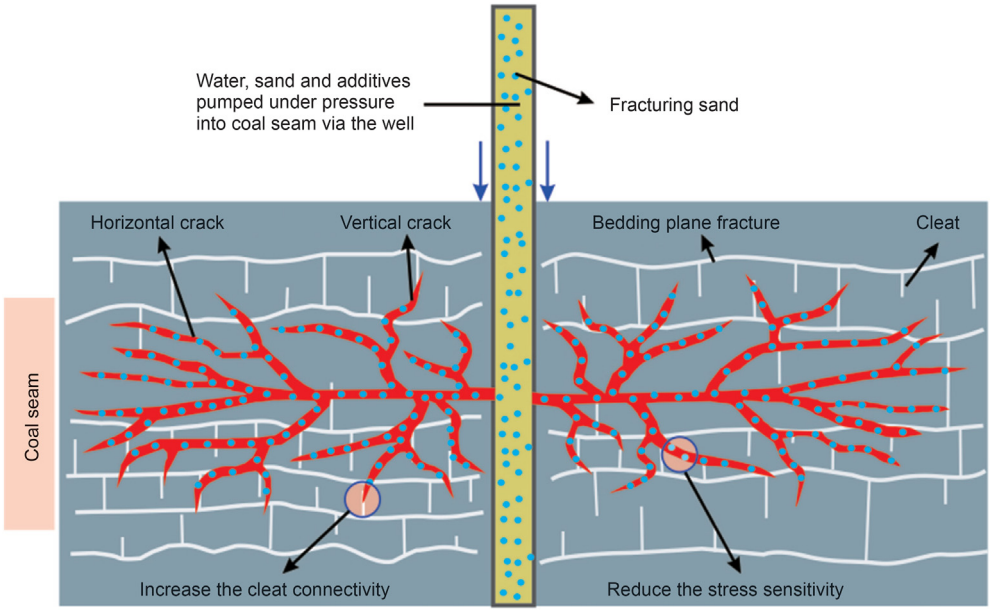


**Fig. 11.** The diagrammatic sketch of enhancing $CO_2$ injectivity for coal reservoir by pre-fracturing.

### 3.4. Comparisons of engineering measures for enhancing $CO_2$ injectivity during $CO_2$-ECBM

Intermittent $CO_2$ injection, $N_2$ displacing $CO_2$ and pre-fracturing are the common engineering measures to improve the $CO_2$ injectivity for the coal reservoir. All of them can amplify the $CO_2$ injection efficiency and injection capacity for $CO_2$-ECBM, however, the improvement level and effect are various. Pre-fracturing is the most efficient measure because it can thoroughly reconstruct the structure of the coal reservoir, which not only improves the three-dimensional permeability immensely but also makes it independent of the influences of effective stress and $ScCO_2$ adsorption. The effect of the intermittent injection is moderate because it can extend the injection process and remedy the reservoir pressure loss during $CO_2$-ECBM, while for an extremely low permeability coal seam, this method may be inefficient. The effect of $N_2$ displacing $CO_2$ is limited, although the permeability will recover to a certain extent, it will attenuate again when $CO_2$ is reinjected, also, it will reduce the sequestration capacity of $CO_2$ and is averse to the geological $CO_2$ sequestration.

The appropriate enhanced injectivity measures should be chosen according to the physical and geological conditions of coal reservoirs. For coal seams with high porosity and high permeability, intermittent $CO_2$ injection or $N_2$ displacing $CO_2$ may be adequate; while for coal seams with low permeability developed in complex geological conditions, these engineering measures need to be combined to obtain an excellent $CO_2$ injection effect.

## 4. Conclusions

The attenuation of $CO_2$ injectivity induced by adsorption swelling restricts the successful launch of $CO_2$-ECBM. In this paper, three commonly-used engineering measures, intermittent $CO_2$ injection, $N_2$ displacing $CO_2$ and pre-fracturing, were simulated by laboratory experiments and their effect and mechanism were clarified and examined. The following conclusions were drawn:

(1) The phase state can affect the intermittent $CO_2$ injection process, for the intermittent $SubCO_2$ injection, the injectivity will reduce to zero within ten injection/stop cycles, while the injection process will last beyond ten injection/stop cycles for intermittent $ScCO_2$ injection. Compared with the continuous injection mode, the net injection volumes of $SubCO_2$ and $ScCO_2$ are improved by 23.80% and 115.11% by using intermittent injection mode. The $CO_2$ injection time is increased by folds and the reservoir pressure loss is complemented in time through intermittent injection mode, thus, the injectivity of $CO_2$ is highly improved.

(2) When $CO_2$ is injected into coal, the adsorption swelling occurs and gradually reaches the maximum value, and the permeability is reduced by 49.42% for $SubCO_2$ and 67.40% for $ScCO_2$. When $N_2$ is injected into coal containing $CO_2$, the gas composition of $CO_2$ decreases and the adsorption swelling recoveries in some degrees, the permeability is increased by 74.82% and 64.95% compared with that in the primary Sub $CO_2$ and $ScCO_2$ injection. The gas composition of $CO_2$, the swelling strain and the permeability all return to the values of those in the primary $CO_2$ injection. $N_2$ injection promotes the matrix shrinking effect induced by the desorption of $CH_4$ and $CO_2$, then the expansion of narrow fractures or reopening of closed fractures causes the increase of $CO_2$ injectivity.

(3) After pre-fracturing treatment, the permeability of the coal sample is averagely advanced by 1–2 orders of magnitude, the irreversible permeability loss rate, average stress sensitivity coefficient and permeability loss rate due to adsorption are averagely lowered by 95.885%, 61.538% and 96.297%, respectively. The permeability of the sample after pre-fracturing is no longer sensitive to the effective stress and $ScCO_2$ adsorption, which is the reason why the injectivity of $CO_2$ has been largely promoted.

(4) The enhanced $CO_2$ injectivity effects of the intermittent $CO_2$ injection, $N_2$ displacing $CO_2$ and the pre-fracturing are various. For the $CO_2$-ECBM project, these engineering measures could be selected individually or jointly to improve the $CO_2$ injectivity, depending on the physical properties and geological conditions of reservoirs.

## Acknowledgments

This work was sponsored by the National Natural Science Foundation of China (Grant nos. 41727801, 41972281, 51979170, 11902208, U1967208 and 41330638), the National Key Research and Development Plan Project of China (2018YFB0605600), the Natural Science Foundation of Hebei Province (E2021210077), the Autonomous subject of State Key Laboratory of Mechanical Behavior and System Safety of Traffic Engineering Structures (ZZ 2020-29) and Science and Technology Research Project of Hebei Province Colleges and Universities (QN2021129).

## References

Ajayi, T., Gomes, J.S., Bera, A., 2019. A review of $CO_2$ storage in geological formations emphasizing modeling, monitoring and capacity estimation approaches. Petrol. Sci. (5–6), 1–36. https://doi.org/10.1007/s12182-019-0340-8.

ASTM D2013. Standard Practice of Preparing Coal Samples for Analysis. Vol. 0vol. 5.06 ASTM International, West Conshohocken, PA.

Bakhshian, S., Hosseini, S.A., Lake, L.W., 2020. $CO_2$-brine relative permeability and capillary pressure of Tuscaloosa sandstone: effect of anisotropy. Adv. Water Resour. 135, 103464. https://doi.org/10.1016/j.advwatres.2019.103464.

Cao, Y., Zhang, J., Zhai, H., Fu, G., Tian, L., Liu, S., 2017. $CO_2$ gas fracturing: a novel reservoir stimulation technology in low permeability gassy coal seams. Fuel 203, 197–207. https://doi.org/10.1016/j.fuel.2017.04.053.

Chao, J., Yu, M., Chu, T., Han, X., Teng, F., Li, P., 2019. Evolution of broken coal permeability under the condition of stress, temperature, moisture content, and pore pressure. Rock Mech. Rock Eng. 52, 2803–2814. https://doi.org/10.1007/s00603-019-01873-x.

Chen, K, Liu, X, Wang, L, 2021. Influence of sequestered supercritical $CO_2$ treatment on the pore size distribution of coal across the rank range. Fuel 306, 121708. https://doi.org/10.1016/j.fuel.2021.121708.

Cheng, P., Yu, Q., 2019. Experimental study on the relationship between the matric potential and methane breakthrough pressure of partially water-saturated shale fractures. J. Hydrol. 578, 124044. https://doi.org/10.1016/j.jhydrol.2019.124044.

Dutta, P., Zoback, M.D., 2012. $CO_2$ sequestration into the Wyodak coal seam of Powder River Basin-Preliminary reservoir characterization and simulation. Int J Greenh Gas Con 9, 103–116. https://doi.org/10.1016/j.ijggc.2012.03.004.

Fan, C., Elsworth, D., Li, S., Chen, Z., Luo, M., Song, Y., Zhang, H., 2019. Modelling and optimization of enhanced coalbed methane recovery using $CO_2/N_2$ mixtures. Fuel 253, 1114–1129. https://doi.org/10.1016/j.fuel.2019.04.158.

Fu, C., Liu, N., 2019. Waterless fluids in hydraulic fracturing-A review. J. Nat. Gas Sci. Eng. 67, 214–224. https://doi.org/10.1016/j.jngse.2019.05.001.

Fujioka, M., Yamaguchi, S., Nako, M., 2010. $CO_2$-ECBM field tests in the Ishikari coal basin of Japan. Int. J. Coal Geol. 82 (3), 287–298. https://doi.org/10.1016/j.coal.2010.01.004.

Gao, J., Xing, H., Turner, L., Steel, K., Sedek, M., Golding, S.D., Rudolph, V., 2017. Pore-scale numerical investigation on chemical stimulation in coal and permeability enhancement for coal seam gas production. Transport Porous Media 116 (1), 335–351. https://doi.org/10.1007/s11242-016-0777-9.

Geng, Y., Tang, D., Xu, H., Tao, S., Tang, S., Ma, L., Zhu, X., 2017. Experimental study on permeability stress sensitivity of reconstituted granular coal with different lithotypes. Fuel 202, 12–22. https://doi.org/10.1016/j.fuel.2017.03.093.

Gunter, W.D., Mavor, M.J., Robinson, J.R., 2005. $CO_2$ storage and enhanced methane production: field testing at Fenn-Big Valley, Alberta, Canada, with application. In: International Conference on Greenhouse Gas Control Technologies, Vancouver, Canada. https://doi.org/10.1016/b978-008044704-9/50042-2.

Huang, J., Hu, G., Xu, G., Nie, B., Yang, N., Xu, J., 2019. The development of microstructure of coal by microwave irradiation stimulation. J. Nat. Gas Sci. Eng. 66, 86–95. https://doi.org/10.1016/j.jngse.2019.03.016.

Ji, X., 2015. Study on Recovery Improvement of CBM Vertical Wells via Hydraulic Fracturing with Nitrogen Injection. Master Thesis. Henan Polytechnic University, Jiaozuo (In Chinese).

Jia, J., Sang, S., Cao, L., Liu, S., 2018. Characteristics of $CO_2$/supercritical $CO_2$

adsorption-induced swelling to anthracite: an experimental study. Fuel 216, 639–647. https://doi.org/10.1016/j.fuel.2017.12.006.
Jiang, C., Duan, M., Yin, G., Wang, J.G., Lu, T., Xu, J., Zhang, D., Huang, G., 2017. Experimental study on seepage properties, AE characteristics and energy dissipation of coal under tiered cyclic loading. Eng. Geol. 221, 114–123. https://doi.org/10.1016/j.enggeo.2017.03.005.
Jin, Y., Liu, X., Song, H., Zheng, J., Pan, J., 2019. General fractal topography: an open mathematical framework to characterize and model mono-scale-invariances. Nonlinear Dynam. 96 (4), 2413–2436. https://doi.org/10.1007/s11071-019-04931-9.
Jin, Y., Wang, C., Liu, S., Quan, W., Liu, X., 2020. Systematic definition of complexity assembly in fractal porous media. Fractals 28 (8), 2050079. https://doi.org/10.1142/S0218348X20500796.
Ju, Y., Wang, J., Wang, H., Zheng, J., Ranjith, P.G., Gao, F., 2016. $CO_2$ permeability of fractured coal subject to confining pressures and elevated temperature: experiments and modeling. Sci. China Technol. Sci. 59 (12), 1931–1942. https://doi.org/10.1007/s11431-016-0478-5.
Kumar, H., Elsworth, D., Liu, J., Pone, D., Mathews, J.P., 2012. Optimizing enhanced coalbed methane recovery for unhindered production and $CO_2$ injectivity. Int J Greenh Gas Con 11 (6), 86–97. https://doi.org/10.1016/j.ijggc.2012.07.028.
Kumar, H., Elsworth, D., Liu, J., Pone, D., Mathews, J.P., 2015. Permeability evolution of propped artificial fractures in coal on injection of $CO_2$. J. Petrol. Sci. Eng. 133, 695–704. https://doi.org/10.1016/j.petrol.2015.07.008.
Li, Q., Wei, Y., Liu, G., Shi, H., 2015. $CO_2$-EWR: a cleaner solution for coal chemical industry in China. J. Clean. Prod. 103, 330–337. https://doi.org/10.1016/j.jclepro.2014.09.073.
Li, C., Zhang, K., Wang, Y., Guo, C., Maggi, F., 2016. Experimental and numerical analysis of reservoir performance for geological $CO_2$ storage in the Ordos Basin in China. Int J Greenh Gas Con 45, 216–232. https://doi.org/10.1016/j.ijggc.2015.11.011.
Li, R., Wang, S., Lyu, S., Xiao, Y., Su, D., Wang, J., 2018. Dynamic behaviours of reservoir pressure during coalbed methane production in the southern Qinshui Basin, North China. Eng. Geol. 238, 76–85. https://doi.org/10.1016/j.enggeo.2018.03.002.
Liu, X, Nie, B, Guo, K, et al., 2021. Permeability enhancement and porosity change of coal by liquid carbon dioxide phase change fracturing. Eng. Geol. 287, 106106. https://doi.org/10.1016/j.enggeo.2021.106106.
Meng, Z., Li, G., 2013. Experimental research on the permeability of high-rank coal under a varying stress and its influencing factors. Eng. Geol. 162, 108–117. https://doi.org/10.1016/j.enggeo.2013.04.013.
Meng, Z., Zhang, J., Wang, R., 2011. In-situ stress, pore pressure and stress-dependent permeability in the Southern Qinshui Basin. Int J Rock Mech Min 48 (1), 122–131. https://doi.org/10.1016/j.ijrmms.2010.10.003.
Niu, Q., Pan, J., Cao, L., Ji, Z., Wang, H., Wang, K., Wang, Z., 2017a. The evolution and formation mechanisms of closed pores in coal. Fuel 200, 555–563. https://doi.org/10.1016/j.fuel.2017.03.084.
Niu, Q., Cao, L., Sang, S., Zhou, X., Wang, Z., Wu, Z., 2017b. The adsorption-swelling and permeability characteristics of natural and reconstituted anthracite coals. Energy 141, 2206–2217. https://doi.org/10.1016/j.energy.2017.11.095.
Niu, Q., Cao, L., Sang, S., Zhou, X., Wang, Z., 2018. Anisotropic adsorption swelling and permeability characteristics with injecting $CO_2$ in coal. Energy Fuel. 32 (2), 1979–1991. https://doi.org/10.1021/acs.energyfuels.7b03087.
Niu, Q., Pan, J., Jin, Y., Wang, H., Li, M., Ji, Z., Wang, K., Wang, Z., 2019a. Fractal study of adsorption-pores in pulverized coals with various metamorphism degrees using $N_2$ adsorption, X-ray scattering and image analysis methods. J. Petrol. Sci. Eng. 176, 584–593. https://doi.org/10.1016/j.petrol.2019.01.107.
Niu, Q., Cao, L., Sang, S., Zhou, X., Liu, S., 2019b. Experimental study of permeability changes and its influencing factors with $CO_2$ injection in coal. J. Nat. Gas Sci. Eng. 61, 215–225. https://doi.org/10.1016/j.jngse.2018.09.024.
Niu, Q., Wang, W., Liang, J., Yuan, W., Wen, L., Chang, J., Ji, Z., Zhou, H., Wang, Z., Jia, X., 2020a. Investigation of the $CO_2$ flooding behavior and its collaborative controlling factors. Energy Fuel. 34, 11194–11209. https://doi.org/10.1021/acs.energyfuels.0c01286.
Niu, Q., Cao, L., Sang, S., Zhou, X., Wang, W., Yuan, W., Ji, Z., Wang, H., Nie, Y., 2020b. Study on the anisotropic permeability in different rank coals under influences of supercritical $CO_2$ adsorption and effective stress and its enlightenment for $CO_2$ enhance coalbed methane recovery. Fuel 262, 116515. https://doi.org/10.1016/j.fuel.2019.116515.
Niu, Q., Cao, L., Sang, S., Wang, W., Zhou, X., Yuan, W., Ji, Z., Chang, J., Li, M., 2021. Experimental study on the softening effect and mechanism of anthracite with $CO_2$ injection. Int. J. Rock Mech. Min. Sci. 138, 104614. https://doi.org/10.1016/j.ijrmms.2021.104614.
Osiptsov, A.A., 2017. Fluid mechanics of hydraulic fracturing: a review. J. Petrol. Sci. Eng. 156, 513–535. https://doi.org/10.1016/j.petrol.2017.05.019.
Oudinot, A.Y., Koperna, G.J., Philip, Z.G., Liu, N., Heath, J.E., Wells, A., Young, G.B., Wilson, T., 2011. $CO_2$ injection performance in the Fruitland coal fairway, San Juan Basin: results of a field pilot. SPE J. 16 (4), 864–879. https://doi.org/10.2118/127073-pa.
Oudinot, A.Y., Riestenberg, D.E., Koperna, G.J., 2017. Enhanced gas recovery and $co_2$ storage in coal bed methane reservoirs with $N_2$ co-injection. Energy Procedia 114, 5356–5376. https://doi.org/10.1016/j.egypro.2017.03.1662.
Pan, Z., Ye, J., Zhou, F., Tan, Y., Connell, L.D., Fan, J., 2017. $CO_2$ storage in coal to enhance coalbed methane recovery: a review of field experiments in China. Int. Geol. Rev. 60 (4), 1–23. https://doi.org/10.1080/00206814.2017.1373607.
Perera, M.S.A., Ranjith, P.G., Viete, D.R., 2013. Effects of gaseous and super-critical carbon dioxide saturation on the mechanical properties of bituminous coal from the Southern Sydney Basin. Appl. Energy 110, 73–81. https://doi.org/10.1016/j.apenergy.2013.03.069.
Ranjith, P.G., Perera, M.S.A., 2011. A new triaxial apparatus to study the mechanical and fluid flow aspects of carbon dioxide sequestration in geological formations. Fuel 90 (8), 2751–2759. https://doi.org/10.1016/j.fuel.2011.04.004.
Reeves, S.R., 2003. Enhanced CBM recovery, coalbed $CO_2$ sequestration assessed. Oil Gas J. 101 (27), 49–53.
Sharma, L.K., Vishal, V., Singh, T.N., 2017. Predicting $CO_2$ permeability of bituminous coal using statistical and adaptive neuro-fuzzy analysis. J. Nat. Gas Sci. Eng. 42, 216–225. https://doi.org/10.1016/j.jngse.2017.02.037.
Shi, Q., Qin, Y., Li, J., Wang, Z., Zhang, M., Song, X., 2017. Simulation of the crack development in coal without confining stress under ultrasonic wave treatment. Fuel 205, 222–231. https://doi.org/10.1016/j.fuel.2017.05.069.
Shi, Q., Qin, Y., Zhou, B., Wang, X., 2019. Porosity changes in bituminous and anthracite coal with ultrasonic treatment. Fuel 255, 115739. https://doi.org/10.1016/j.fuel.2019.115739.
Singh, H., 2018. Impact of four different $CO_2$ injection schemes on extent of reservoir pressure and saturation. Adv Geo-Energy Res. 2 (3), 305–318. https://doi.org/10.26804/ager.2018.03.08.
Tan, Y., Pan, Z., Liu, J., Wu, Y., Haque, A., Connell, L.D., 2017. Experimental study of permeability and its anisotropy for shale fracture supported with proppant. J. Nat. Gas Sci. Eng. 44, 250–264. https://doi.org/10.1016/j.jngse.2017.04.020.
van Bergen, F., Krzystolik, P., van Wageningen, N., Pagnier, H., Jura, B., Skiba, J., Winthaegen, P., Kobiela, Z., 2009. Production of gas from coal seams in the Upper Silesian Coal Basin in Poland in the post-injection period of an ECBM pilot site. Int. J. Coal Geol. 77 (1), 175–187. https://doi.org/10.1016/j.coal.2008.08.011.
Wang, Z., Pan, J., Hou, Q., Yu, B., Li, M., Niu, Q., 2018a. Anisotropic characteristics of low-rank coal fractures in the Fukang mining area, China. Fuel 211, 182–193. https://doi.org/10.1016/j.fuel.2017.09.067.
Wang, Z., Pan, J., Hou, Q., Niu, Q., Tian, J., Wang, H., Fu, X., 2018b. Changes in the anisotropic permeability of low-rank coal under varying effective stress in Fukang mining area, China. Fuel 234, 1481–1497. https://doi.org/10.1016/j.fuel.2018.08.013.
Wang, Z., Deng, Z., Fu, X., Li, G., Pan, J., Hao, M., Zhou, H., 2020a. Effects of methane saturation and nitrogen pressure on $n_2$-enhanced coalbed methane desorption strain characteristics of medium-rank Coal. Nat. Resour. Res. https://doi.org/10.1007/s11053-020-09783-4.
Wang, R., Wang, Q., Niu, Q., Pan, J., Wang, H., Wang, Z., 2020b. $CO_2$ adsorption and swelling of coal under constrained conditions and their stage-change relationship. J. Nat. Gas Sci. Eng. 76, 103205. https://doi.org/10.1016/j.jngse.2020.103205.
Wei, M., Liu, J., Elsworth, D., Li, S., Zhou, F., 2019. Influence of gas adsorption induced non-uniform deformation on the evolution of coal permeability. Int J Rock Mech Min 114, 71–78. https://doi.org/10.1016/j.ijrmms.2018.12.021.
Wong, S., Law, D., Deng, X., Robinson, J., Kadatz, B., Gunter, W.D., Jianping, Y., Sanli, F., Zhiqiang, F., 2007. Enhanced coalbed methane and $CO_2$ storage in anthracitic coals-Micro-pilot test at South Qinshui, Shanxi, China. Int J Greenh Gas Con 1 (2), 215–222. https://doi.org/10.1016/S1750-5836(06)00005-3.
Wu, Y., Pan, Z., Zhang, D., Down, D.I., Lu, Z., Connell, L.D., 2018. Experimental study of permeability behaviour for proppant supported coal fracture. J. Nat. Gas Sci. Eng. 51, 18–26. https://doi.org/10.1016/j.jngse.2017.12.023.
Xu, L., Myers, M., Li, Q., White, C., Zhang, X., 2020. Migration and storage characteristics of supercritical $CO_2$ in anisotropic sandstones with clay interlayers based on X-CT experiments. J. Hydrol. 580, 124239. https://doi.org/10.1016/j.jhydrol.2019.124239.
Yamazaki, T., Aso, K., Chinju, J., 2006. Japanese potential of $CO_2$ sequestration in coal seams. Appl. Energy 83 (9), 911–920. https://doi.org/10.1016/j.apenergy.2005.11.001.
Ye, Z., Zhang, L., Hao, D., Wang, C., 2017. Experimental study on the response characteristics of coal permeability to pore pressure under loading and unloading conditions. J. Geophys. Eng. 14, 1020–1031. https://doi.org/10.1088/1742-2140/aa7033.
Yun, J., Xu, F., Liu, L., Zhong, N., Wu, X., 2012. New progress and future prospects of CBM exploration and development in China. Int J Min Sci Technol 22 (3), 363–369. https://doi.org/10.1016/j.ijmst.2012.04.014.
Zhang, Z., Huisingh, D., 2017. Carbon dioxide storage schemes: technology, assessment and deployment. J. Clean. Prod. 142, 1055–1064. https://doi.org/10.1016/j.jclepro.2016.06.199.
Zhang, J., Liu, K., Clennell, M.B., Dewhurst, D.N., Pan, Z., Pervukhina, M., Han, T., 2015. Molecular simulation studies of hydrocarbon and carbon dioxide adsorption on coal. Petrol. Sci. 12 (4), 692–704. https://doi.org/10.1007/s12182-015-0052-7.
Zhang, X.G., Ranjith, P.G., Li, D.Y., Perera, M.S.A., Ranathunga, A.S., Zhang, B.N., 2018. $CO_2$ enhanced flow characteristics of naturally-fractured bituminous coals with $N_2$ injection at different reservoir depths. J $CO_2$ Util. 28, 393–402. https://doi.org/10.1016/j.jcou.2018.11.001.
Zhao, Y., Yu, Q., 2017. $CO_2$ breakthrough pressure and permeability for unsaturated low-permeability sandstone of the Ordos Basin. J. Hydrol. 550, 331–342. https://doi.org/10.1016/j.jhydrol.2017.04.050.
Zhi, S., Elsworth, D., Liu, L., 2019. W-shaped permeability evolution of coal with supercritical $CO_2$ phase transition. Int. J. Coal Geol. 211, 103221. https://doi.org/10.1016/j.coal.2019.103221.
Zhou, J., Liu, M., Xian, X., Jiang, Y., Liu, Q., Wang, X., 2019. Measurements and

modelling of $CH_4$ and $CO_2$ adsorption behaviors on shales: Implication for $CO_2$ enhanced shale gas recovery. Fuel 251, 293–306. https://doi.org/10.1016/j.fuel.2019.04.041.

Zhou, J., Tian, S., Zhou, L., Xian, X., Yang, K., Jiang, Y., Zhang, C., Guo, Y., 2020. Experimental investigation on the influence of sub- and super-critical $CO_2$ saturation time on the permeability of fractured shale. Energy 191, 116574. https://doi.org/10.1016/j.energy.2019.116574.

Zou, J., Chen, W., Yang, D., Yu, H., Yuan, J., 2016. The impact of effective stress and gas slippage on coal permeability under cyclic loading. J. Nat. Gas Sci. Eng. 31, 236–248. https://doi.org/10.1016/j.jngse.2016.02.037.